

Development of eco-friendly brake pads using oil residue materials: Assessment of mechanical properties, biodegradation, and environmental impact

Sunil Kumar Hemanth M^{1*} and Edwin Raja Dhas J²

¹Research Scholar, Department of Mechanical Engineering, Noorul Islam Centre for Higher Education, Kumaracoil, Tamil Nadu, India.

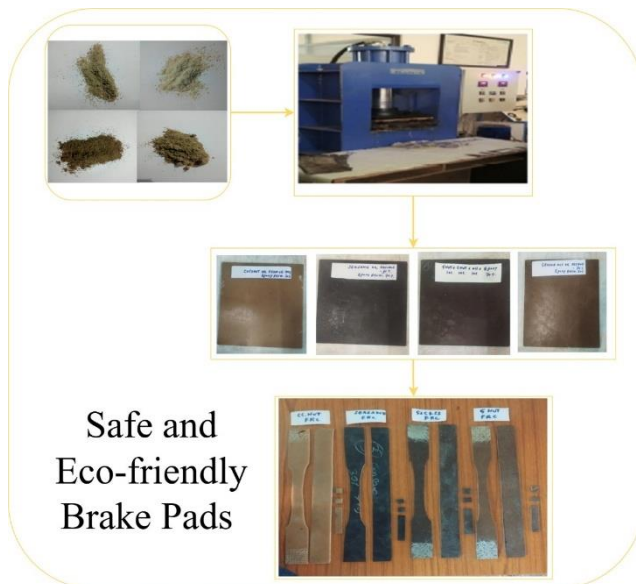
²Head of the Department, Department of Automobile Engineering, Noorul Islam Centre for Higher Education, Kumaracoil, Tamil Nadu, India.

Received: 22/02/2025, Accepted: 25/03/2025, Available online: 25/04/2025

*to whom all correspondence should be addressed: e-mail: sunilkumarhemanth@outlook.com

<https://doi.org/10.30955/gnj.07399>

Graphical abstract



Abstract

Brake pads are the major automotive component that ensures safe braking by controlling the speed of vehicles. Conventional brake pads contain harmful materials like asbestos and heavy metals, adversely affecting human health and the environment. Conventionally, there is an increasing demand for eco-friendly alternatives to maintain or improve the performance of brake pads with reduced environmental impact. In this study, oil residual materials from coconut, groundnut, and sesame, as well as a composite blend of these three residues, were used to create environmentally friendly brake pads. The performance of these residues combined with an epoxy resin matrix with a reinforcement ratio of 30:70 is evaluated. Various mechanical properties like tensile, impact, hardness, flexural strength, wear test, chemical properties like FTIR, water absorption, thermal analysis as TGA, microstructure test of SEM & EDS, and biodegradation test with bacteria as *Acinetobacter baumannii* compost

and its morphological surface are examined for assessing the environmental impact of these materials. The results demonstrated notable improvements with mechanical properties and biodegradation analysis, confirming these materials' environmental sustainability and highlighting their potential to be utilized as an effective reinforcement in brake pad applications. Flexural strength improved by 15-20%, with values of about 42.5 MPa, while tensile strength rose by around 18-22%, reaching up to 28.6 MPa. The impact strength was increased by 25-30%, and energy absorption reached 4.9 kJ/m², higher than the 3.7 kJ/m² achieved by conventional alternatives. Superior abrasion performance was shown by an 8-10% rise in Shore D hardness, which reached values of 79-81, and an improvement in wear resistance, with a specific wear ratio decrease of 12-16%.

Keywords: Brake Pads, Automotive, Oil Residue, Mechanical Properties, Biodegradation, Microstructure.

1. Introduction

Brake pads are the most important component of automobile braking systems since they are responsible for the safe deceleration and stopping of vehicles by generating friction against the brake rotors (Ammar *et al.* 2023). Traditional brake pads integrate asbestos, heavy metals, and other harmful substances, posing serious health and environmental threats. More likely, asbestos causes severe respiratory issues and cancers such as mesothelioma, while heavy metals like copper and lead subsidize environmental pollution and toxicity in aquatic ecosystems. With the increasing consciousness of these threats, the automotive industry is under pressure to develop eco-friendly brake pads that could match or exceed the performance of traditional materials deprived of the related risks (Dharmakrishnan *et al.* 2022).

Eco-friendly brake pads utilize sustainable and non-toxic materials, including organic fibers, ceramics, and various biodegradable composites (Irawan *et al.* 2022). These substitutes aim to reduce harmful emissions during

production and use and improve the overall sustainability of automotive parts. For instance, some research has focused on incorporating agricultural waste, such as coconut fibers and snail shells, which are abundant and renewable, into brake pad formulations. These materials offer promising mechanical properties like improved wear resistance and thermal stability, which are essential for effective braking performance. Developing these green materials also aligns with global efforts to minimize automotive pollution and promote environmental sustainability (Naidu *et al.* 2022). As regulatory standards become more stringent, eco-friendly brake pads can help manufacturers comply with environmental regulations and reduce their carbon footprint. Overall, the shift towards sustainable brake pad materials represents a significant advancement in automotive technology, addressing environmental concerns and the demand for high-performance, safe braking systems (Sutikno *et al.* 2018). Oil residues, typically regarded as waste products, have recently garnered attention as potential raw materials for various applications, including the production of brake pads (Balakrishnan *et al.* 2019). These residues are by-products of oil refining and are often disposed of through environmentally harmful methods such as incineration or landfill. Utilizing oil residues in brake pad production offers a sustainable waste management solution and a cost-effective alternative to traditional materials (Kumar *et al.* 2022). The specific oil residues investigated in this study include those derived from various industrial processes. These residues possess unique physical and chemical properties that may render them suitable for use in brake pads. The feasibility of oil residues for this application is assessed based on a comprehensive analysis of their mechanical, chemical, and biodegradation properties. Nandiyanto *et al.* (2024) specifically investigated teak sawdust and clamshell powder mixed with epoxy resin for brake pad fabrication. Various compositions were tested for performance using compression, friction, and puncture tests, revealing optimal strength and balance with a teak sawdust and clamshell blend. Singh (2024) analyzed different ratios of cement dust and barium sulfate using a Krauss machine and showed the best performance by composites with 30% cement dust and 20% barium sulfate, having low wear and high friction. Kunaroop *et al.* (2024) focussed on developing polybenzoxazine friction composites free from asbestos and copper, incorporating different proportions of synthetic graphite and carbonized hemp hurd (CHH). The thermal, mechanical, and tribological characteristics were assessed, demonstrating that higher CHH enhances the strength, modulus, and wear resistance. Khafidh *et al.* (2023) used the hand layup method to fabricate composite brake pad materials using epoxy resin as the matrix and rice husk, Al_2O_3 , and Fe_2O_3 as reinforcing materials. Density, hardness, thermal analysis, flexural strength, TGA/DSC, and SEM are included as characterization tests, and wear testing demonstrates improved mechanical properties with increased reinforcement percentages, highlighting the method's viability and contribution to sustainable automotive applications.

Eziwhuo *et al.* (2023) utilized oyster sea shells (OSS) and coconut fruit fibers (CFF) as a substitute for asbestos. Prepared in three levels with additives like phenolic resin and graphite, molded using Box Behnken Design. Wulansari *et al.* (2024) investigated the tensile strength and analyzed the surface and degree of dwelling, focusing on clamshells with calcium carbonate, cardboard waste, and orange peel cellulose. The results obtained a maximum tensile strength of 6.521 MPa. Ekpruke *et al.* (2023) analyzed the morphological and tribological factors to investigate brake pad properties developed from Thais Coronata seashell wastes with reinforcement materials. The chemical composition was determined using EDX analysis, showing the presence of toxic heavy materials in the two commercial brake pads. Naidu *et al.* (2022) discussed the friction and wear analysis of hemp fibers using ANOVA. The results showed a lowered wear rate and a good coefficient of friction. Zhiqiang Wang *et al.* (2024) suggested the Investigation of the Interconnected and Synergistic Relationship Between the Ecological Environment and Economic Development in China and Its Temporal and Spatial Evolution. The greatest coupling coordination in 2022 was in Guangdong Province (0.99), while the quickest yearly growth rate was in Gansu Province (13.4%). Continually, the disparity between the relative levels of coupling and coordination across the provinces is decreasing. Baoshuai Yao *et al.* (2024) proposed the analysis of the Dynamic Evolutionary Game and the Impact of Green Taxation on Advancing the New Energy Sector. This study verifies that green taxation substantially advances the growth of China's new energy sector. It is practical and important to promote robust growth in this sector while also aiding in reducing regional industrial development disparities via tax policy. Tong L *et al.* (2024) discussed the Influence of China's Digital Economy on Farming Carbon Emissions. The growth of a region's digital economy will dampen the intensity of carbon emissions from agriculture in nearby provinces due to the geographical spillover effect of digital economic development. In light of this, measures to decrease farming carbon emissions, encourage the synchronized growth of the digital economy in the area, and fortify the building of digital infrastructure are all being considered. Zou F *et al.* (2024) presented the Technological Innovation and Ecological Regulation Decrease Carbon Dioxide Emissions. Using variance decomposition, the author examined how each new interest shock affected changes in industrial TI, environmental regulations, and CO_2 emissions. As a resource for appropriate departments working to develop emission decrease policies and industrial technological innovation, this study enhances the application of institutional theory and technical innovation theory to reduce CO_2 emissions. Yang Su *et al.* (2024) introduced the interactive effects of agricultural carbon emission efficacy and novel urbanization. According to the study's findings, (1) broad assumptions about the association between urbanization and agricultural carbon emission efficacy are incorrect; urbanization improves agricultural carbon emission efficacy. The Granger causal connection between agricultural urbanization and farming carbon emission

efficiency holds in both primary grain-producing and secondary grain-producing regions; however, new urbanization has a far more formidable inhibitory effect on improving primary grain-producing regions' carbon emission efficiency.

Liqin Wen *et al.* (2024) deliberated on the coupled and coordinated improvement of Shanxi Province tourism, urbanization, and environmental environment. The findings reveal that from 2012 to 2022, tourism, urbanization, and natural environment saw rising comprehensive development levels. However, system coupling and synchronization degrees were low, indicating dysfunctional states and urbanization levels remained greater than tourism and biological environment improvement levels. Wang Z *et al.* (2024) examined the Carbon Emission Peaks in Large Energy Production Region. The closed STIRPAT model overestimates carbon emissions by 20%-44% and delays the year of peak carbon in Shanxi compared to the open STIRPAT model. As a result, while planning its carbon emission strategy, Shanxi should consider the national push for energy efficiency as a key limitation for the province's peak carbon policy and work to create a carbon emission peaking program that can adapt to changing circumstances. Wang C *et al.* (2024) analyzed the impact of digital financial inclusion on agricultural carbon emission. For China's agricultural sector to attain low-carbon and sustainable development, it must prioritize the multi-faceted improvement of digital technology facilities, the development of digital financial inclusion, and the upgrading of agricultural industrial structures. These efforts will help promote a greener, more environmentally friendly agricultural transformation and significantly reduce agricultural carbon emissions. Wu Q *et al.* (2024) recommended the Effects on high-quality urban economic growth of low-carbon and creative city pilot programs. Examining heterogeneity revealed that the dual-pilot strategy had a stronger impact on promoting high-quality economic growth in large-scale, non-resource-based, and eastern cities. Promoting high-quality development of the urban economy necessitates that the government maintain its support for and optimization of the dual-pilot policy, fully utilize policy synergies, and rationally and scientifically plan the policy layout according to the city's characteristics.

Liqin Wen *et al.* (2025) suggested the Environmental Regulation's Effect on Green Innovation in Regional Cross-Border E-Commerce. By analyzing the effects of environmental regulations on the connection between EGIE promotion and pollution management, this research hopes to provide the groundwork for future decisions about the coordinated growth of regional cross-border e-commerce and environmental protection. Liqin Wen *et al.* (2024) proposed the Changing Consumer and Producer Behavior in Response to the Double Subsidy Policy and Their Choice of Environmentally Friendly Strategies. The simulation experiment's findings reveal that a system's overall propensity to shift toward green production and consumption positively correlates with the initial propensity of both enterprises and consumers toward

green consumption. A combination of purchase and production subsidies allows the government to accelerate the system's steady-state approach compared to using only one subsidy mechanism. Simultaneously, changes in the pricing of various refrigerator kinds might impact the system's evolution strategy in various ways. Keyong Zhang *et al.* (2024) introduced the Effects of Manufacturing Green Technology Innovation on the Sector's High-Quality Growth Within the Context of "Dual Circulation." Green technological innovation positively impacts the manufacturing industry's internal cycle, which fosters high-quality enhancement. Green technological innovation can drive the internal cycle, promoting high-quality development within the industry.

Liqin Wen *et al.* (2024) presented the impact of the online reputation of news presenters on customers' willingness to buy within the framework of the digital economy. The findings indicate that the credibility of Internet celebrity hosts significantly affects customers' propensity to buy on international live-streaming e-commerce platforms. Mediating the relationship between customers' propensity to buy and the reputation of Internet celebrity anchors, initial trust accounts for 73.59% of the entire impact. Additionally, gender moderates the associations between customers' initial trust and buy inclination. Yaolei Li *et al.* (2024) suggested examining the four-way game between developers and manufacturing businesses that depend on industrial internet platforms for transformation and upgrading. According to research, government subsidies and fines impact manufacturing businesses, platforms, and developers' strategic decisions. Platform and developer long-term collaboration and steady development may be achieved with a fair revenue-sharing contract coefficient. Theoretically, manufacturing businesses, industrial Internet platforms, governments, and developers may use the established effective range of influencing elements to guide strategy choices as the system evolves to various stable states.

Danhong Shen *et al.* (2024) proposed the Integrated and Coordinated Growth of Green Finance and Climate Investment. The eastern coastal area is on the brink of dislocation and has the greatest coupling coordination level. Additionally, the Northwest area is experiencing considerable dislocation and has the lowest degree of coordination. Given these results, China's green finance and climate investment policies may be better planned and implemented. Hongjun Zeng *et al.* (2025) recommended the Large US technology companies and the green finance index: tail risk contagion and multiscale spillovers. The empirical results have practical relevance for diverse market players worried about green financing and high-tech asset risks across various periods and market situations. Weifeng Xia *et al.* (2025) presented the digital economy enhances carbon emission efficiency. According to the empirical evidence, a higher degree of digital economic growth is associated with substantially improved carbon emission efficiency. The conclusion holds up even after many stability tests. There are large regional differences, but the digital economy as a whole has been

growing at a steady clip. According to heterogeneity research, carbon emission performance may be substantially enhanced by the digital economy in eastern cities, cities with plentiful human capital, and cities with minimal budgetary pressure.

Kumaravel *et al.* (2024) suggested the combustion endoscopy to explore the flame characteristics of gasoline engines fuelled by gasoline-pentanol blends. Increasing the percentage of Pentanol in the gasoline improved the engine's performance. At full load, the BTE of the gasoline mix with 30% pentanol was 5.71 percent more than gasoline alone. At the same time as NO emissions rose, emissions of CO and HC fell. The findings of the tests show that engines can run on up to 30% Pentanol with no changes made to the fuel mixture. Saravanan *et al.* (2024) proposed that A spark-ignition engine with a high-insulation coating on the piston crown burns a mixture of gasoline and lemon peel oil. There was a 3% improvement in thermal efficiency for the coated piston engine running on a 20% mix of lemon peel oil and a 4.69% improvement for the uncoated piston running on pure gasoline. Compared to the engine running on gasoline with an uncoated piston, the engine running on a 20% mix of lemon peel oil with a coated piston reduced hydrocarbon emissions by 12.7% and carbon monoxide emissions by 12%, respectively. Haiter Lenin Allasi *et al.* (2023) recommended the impact of synthesized cerium oxide nanoparticles with neem (*Azadirachta indica*) oil biofuel. An environmentally friendly synthesis method is used to produce cerium oxide nanoparticles. To test the additives' effects, four different fuel samples were prepared: (i) pure biodiesel (PB), (ii) biodiesel with 100 ppm ceO₂, (iii) biodiesel with 90% ethanol and 10% BE, and (iv) biodiesel with 100 ppm ceO₂ and 10% BCeE. Fuel BCeE outperforms its counterparts experimentally, thanks to its oxygen buffering properties and the additives' atomization enhancement.

Haiter Lenin *et al.* (2024) introduced the Bio-Filler Effects on Luffa Acutangula Fiber Reinforced Polymer Composite Properties and the Taguchi Method for Parametric Optimization. Compared to composites devoid of wood dust, those containing 20% wood dust show considerable improvements in mechanical characteristics, including a flexural strength increase of 48.78%, an impact strength of 54.64%, and a tensile strength of 17.56%. Results like this highlight the possibility of bio-filled LAF composites for lightweight structural uses in environmentally conscious and mechanically demanding industries like aerospace and automotive. Sujin Jose Arul *et al.* (2024) presented the effect of surface chemical actions on mechanical characteristics and wear ratio of epoxy polymer amalgams reinforced with Beerakaya (*Luffa acutangula*). According to the study, the mechanical elements of Luffa acutangula fiber amalgams may be improved by chemically treating triple fiber layers and treating the fiber surfaces. Scanning electron microscopy was also used to assess the treated fiber composites' broken surfaces. In sum, the findings of this study provide the groundwork for a natural fiber composite that is both sustainable and kind to the

environment; it may even one day replace synthetic materials. A., HAITER LENIN *et al.* (2024) discussed the An Empirical Investigation into the Wear Analysis of a Cu-Ni-Sn Hybrid Composite for Multi-Functional Applications with Nano B. Scanning electron microscopy pictures are utilized to analyze the surface's microstructure and morphology that has been worn. The lower number of holes in the hybrid composite causes a decrease in sintered density, which condenses material defects.

The main contributions of the study are as follows:

To evaluate the performance of four different materials derived from oil residues for their potential application in brake pads.

To examine the mechanical and chemical properties of brake pad applications.

To determine the biodegradation properties and to investigate the morphological and compositional features.

2. Materials and Methods

2.1. Engineering materials

Using natural fibers in the formulation of brake pads offers several advantages, including reduced environmental impact, enhanced thermal stability, and improved friction performance. This study uses eco-friendly materials, including oil cake residues of coconut oil, sesame oil, and groundnut oil, for efficient brake pad materials that meet the rigid performance requirements of modern automotive applications. These ingredients, eliminated from associated oil extraction plants, are collected and ground into powders in a flour mill to use as reinforcement as fillers in mixtures. The fiber material components, Sesame oil residue (SOR), coconut oil residue (COR), Groundnut oil residue (GOR), and a combination of coconut, groundnut, and sesame (CGS) oil residues are taken for consideration for investigating the feasibility of oil residue materials for brake pads. The oil residue images are illustrated in **Figure 1**. Due to their availability and fiber content, additional natural fibers and oil remnants such as rice husks, palm kernel shells, jatropha residues, and sunflower husks were investigated during the first experiments. Their worse compatibility with the epoxy matrix, variable particle shape, and less-than-ideal thermal or mechanical qualities noted during trial blending and testing were the main reasons they were not chosen for the final formulation. For example, the flexural and tensile strengths of residues made from rice husks and palm kernels were lower because of the weak interfacial bonding and uneven particle distribution. Residues with a greater ash content and lower biodegradation rates may impact the stability of performance and environmental sustainability. The mechanical and ecological performance goals in brake pad applications might be better met using residues from coconuts, groundnuts, and sesame seeds because of their better balance of structural reinforcement, heat resistance, homogenous dispersion, and biodegradability.

2.2. Specimen preparation

The reinforcement fiber materials are used with an epoxy resin matrix in a ratio of 30:70. The amount of

reinforcement (in percentage) and the powder weight are given in **Table 1**. The ingredients are mixed with the help of compression molding, shown in **Figure 2**, with a die size of 300 mm x 300 mm, suitable for precise molding in various applications. Featured with 3 mm & 5 mm plate thickness options, offering versatility in processing materials. The system operates up to 400 bar maximum pressure and maximum temperature of 400°C for robust thermal performance. Reinforcing materials made from coconut, groundnut, and sesame residues improve brake pad performance without negatively impacting the environment because of their special blend of mechanical, thermal, and biodegradability characteristics. The high tensile strength, impact resistance, and wear endurance provided by these residues' abundance of lignocellulosic fibers are crucial for brake applications. Brake fade is less likely to occur because of their built-in thermal stability, which protects them from deterioration at normal braking temperatures. Additionally, these agro-waste products are renewable, inexpensive, and readily accessible, so they may replace traditional fillers made of asbestos or synthetic materials. Reducing friction-induced wear and noise, the oil content in these residues also helps with increased lubrication. Composting tests have shown their biodegradability, further improving environmental

compatibility and minimizing their long-term ecological effect.



Figure 1. Oil residue images



Figure 2. Compression molding

Table 1. Preparation of test specimen

SL. NO	Matrix	Reinforcement	Percentage			Powder Weight
			Coconut	Sesame	Ground Nut	
1	Epoxy Resin	Coconut oil residue	15%	-	-	45g+15-60g
2	Epoxy Resin	Sesame oil residue	-	15%	-	45g+15-60g
3	Epoxy Resin	Ground Nut oil residue	-	-	15%	45g+15-60g
4	Epoxy Resin	Combined oil residue	5%+5%+5% Total=15%	-	-	20g+20g+20g+60g

Table 2. Specimen preparation

SL. NO	Matrix	Reinforcement	Specimen preparation
1	Epoxy Resin	Coconut oil residue	Tensile test-1 Nos
2	Epoxy Resin	Sesame oil residue	Flexure charges-1 Nos
3	Epoxy Resin	Ground Nut oil residue	Hardness test (HRM SCALE)-1 Nos
4	Epoxy Resin	Combined oil residue	Wear test-1 Nos impact test-1 Nos

This study used matrix material and epoxy resin reinforced with different oil residues to achieve a 15% reinforcement percentage. The sample's COR, SOR, and GOR portions are used in a proportion of 15%, particularly 45g of epoxy resin combined with an additional 15-60g of oil residues. The combined oil residue includes 5% of individual oil residues, resulting in 15% reinforcement and 20g of each oil residue mixed with 60g of epoxy resin. The number of specimens prepared for various tests in this study is given in **Table 2**. The manufactured specimens in solid form are illustrated in **Figure 3**. For a more thorough assessment of the materials' degrading behavior, it would be beneficial to do tests with other microbial species like *Bacillus subtilis*, *Pseudomonas aeruginosa*, or fungal strains like *Aspergillus niger*. Natural exposure scenarios, soil burial, and aqueous

media are some environmental variables that will be tested for biodegradation in future research. This will help to replicate real-world settings as closely as possible.

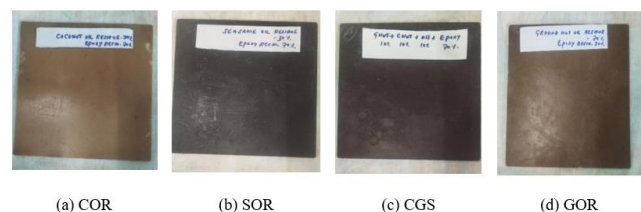


Figure 3. The solid form of specimens.

Specimens are prepared to evaluate the mechanical and biodegradation elements of the reinforced materials. The standard dimension utilized for preparing the specimen is based on the ASTM D638 standard, outlining the

dimensions and specifications for the testing mechanical properties as in **Figure 4**. Potential variables that might affect the results of mechanical properties include changes in sample preparation, such as unequal compaction pressure during molding, slightly different curing times, and inconsistent mixing of oil residual components and epoxy resin. It has also been recognized that data accuracy relies heavily on the precision and calibration status of testing equipment, such as the TGA analyzer, tribometer, Shore D hardness tester, and Universal Testing Machine **Table 3**. Dimension of specimens

Feature	Dimension (mm)	Description
Overall Length	145	Total length of the specimen from end to end
Gauge Length	80	Length of the narrow section where measurements are taken
Narrow Section Width	20	Width of the central narrow section for stress concentration
Fillet Radius	22.5	The radius of the fillet connecting narrow section to wider ends
Thickness	3	Uniform thickness throughout the specimen

Table 4. Machine setting and test parameters for wear testing

Specimen	Test variables			Machine setup			
	Applied Loads (N)	Sliding Distance (m)	Sliding velocity (m/sec)	Sliding dia in mm	RPM	Period in secs	Period in min
A	10	500	1	40	478	500	8.332
B	10	500	1	40	478	500	8.332
C	10	500	1	40	478	500	8.332
D	10	500	1	40	478	500	8.332

3. Evaluation of mechanical properties

Specimens are reinforced to analyze the tensile strength using tensile test, bending strength using the flexure test, hardness using the HRM scale, abrasion resistance using the wear test, and gauge impact resistance using the impact test. **Figure 5** denotes the prepared specimen in ASTM D638 standard for evaluating various mechanical properties. Coconut, groundnut, and sesame oil wastes are inexpensive agricultural by-products that may be obtained for as little as \$0.30 to \$0.50 per kilogram, which is far less expensive than traditional metallic or asbestos-based fillers. Even while it's still within an industrially acceptable range, the epoxy resin that acts as the matrix somewhat increases the overall cost. There is an estimated 25-30% reduction in the overall manufacturing cost per unit of brake pads compared to traditional pads. Compression molding and curing, two common composite fabrication processes, provide the basis of the scalable production process and may be easily integrated into preexisting manufacturing infrastructure with little to no modification. The produced environmentally friendly brake pads also outperform commercially available non-asbestos organic (NAO) pads in terms of mechanical performance, which includes tensile strength, wear resistance, and thermal stability. In addition to being better options from an environmental standpoint, these materials can biodegrade and do not contain any harmful components.

3.1. Tensile strength testing

Tensile strength evaluation confirms that the brake pads can sustain the mechanical and thermal loads encountered during braking without failure, which assures structural veracity, safety, and resilience under stress (Yigrem *et al.*

(UTM). Test conditions, including air temperature and relative humidity, have been considered. This is especially true for water absorption and biodegradation experiments. The specimen's dog-bone shape ensures uniform stress distribution during testing. The key measurements are tabulated in **Table 3**. These dimensions facilitate accurate and reliable data acquisition regarding tensile strength and modulus of elasticity.

2022). Additionally, it promises that the performance of recycled materials using oil residues is not compromised. Tensile strength testing is necessary for producing reliable and eco-friendly automotive components since it aids in quality control, selection of materials, and brake pad longevity. The tensile tests are implemented using the FIE-F-100, C-UTM-calibration model. The Halpin-Tsai model evaluates composite materials' mechanical properties, especially reinforced with fibers (Hemlata and Maiti 2015). It estimates the tensile strength of the composite materials. The modified Halpin-Tsai equation to predict the tensile strength is given by Equation (1)

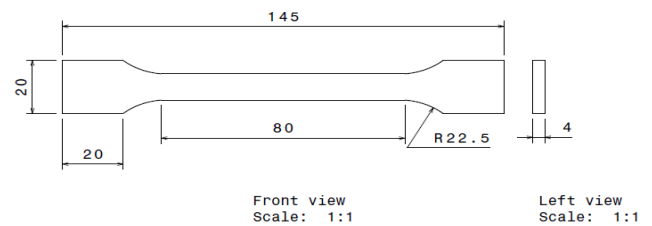


Figure 4. Dimensions with ASTM D638 standard

$$S_C = S_f \cdot V_f + S_m \cdot V_m \quad (1)$$

where, S_C is the tensile strength of the composite, which is calculated by the weighted sum of fiber tensile strength S_f and matrix tensile strength S_m . The volume fraction of fiber (V_f) and matrix (V_m) is denoted by the Equation (2).

$$V_f + V_m = 1 \quad (2)$$

3.2. Wear strength testing

A pin-on-disk method is a standardized tribological method for evaluating the materials' wear and frictional behavior.

Sliding wear under controlled conditions is simulated using a stationary pin pressed against a rotating disk. The pin and disk's volume loss are separately calculated to evaluate the wear. The pin has a spherical end, and the disk has a flat surface; the volume loss for the pin is given in Equation 3.

$$V_p = \frac{\pi \left(\frac{d}{2}\right)^4}{64R} \quad (3)$$

where R is the radius, and d is the wear scar diameter of the pin. The geometric relations for the volume loss of the pin are depicted in Equation 4.

$$V_p = \frac{\pi h}{6} \cdot \left[\frac{3d^2}{4} + h^2 \right] \quad (4)$$

where h is defined as Equation 5,

$$h = r - \sqrt{r^2 - \frac{d^2}{4}} \quad (5)$$

The volume loss of the disc with a wear track having minimal pin wear is given by Equation 6.

$$V_d = \frac{\pi \cdot R \cdot (w)^3}{6r} \quad (6)$$

where R and w are the wear track radius and width, respectively, and r is the radius of the spherical end of the pin. The geometric relations for the volume loss of the disc are depicted in Equation 7.

$$V_d = 2\pi R \cdot \left[r^2 \sin^{-1} \left(\frac{d}{2r} \right) - \frac{d}{4} \sqrt{4r^2 - d^2} \right] \quad (7)$$

Table 4 represents the test parameters used for wear testing. Mechanical parameters (hardness, flexural strength, tensile strength, and impact resistance) were compared among groundnut, coconut, and sesame-based composites using one-way analysis of variance. The findings supported statistically significant variations ($p < 0.05$) in critical parameters, further demonstrating that the kind of filler affects the performance of the composite. Also, this study used Pearson's correlation analysis to examine how mechanical, biodegradation and thermal properties were related; this study found that filler dispersion positively correlated with biodegradation rate and thermal stability.



Figure 5. Specimens in ASTM D638 standard

3.3. Hardness testing

The hardness of the material is obtained using the Rockwell hardness testing, where the 'M' scale is designed to measure the hardness of the softer materials. The Rockwell hardness estimates depth of penetrations of indenters under a large load compared to that under minor loads. Here, the M scale employs a ball indenter with a major load of 100kgf. Ensuring that the sample's surface is smooth, flat, and free of debris, it is mounted on the test machine with a ball indenter with a diameter of 1.588mm and a major load of 100kgf for measuring the penetration depth. These measurements are used to determine the Rockwell Hardness Number (HRM), which is calculated using Equation 8.

$$HR_M = N - \frac{h - h_0}{0.002} \quad (8)$$

where N represents the hardness number as read directly from the scale, h , and h_0 is the depth of penetration under major and minor loads, respectively. The Brinell Hardness Number (BHN) measures material hardness derived from the Brinell hardness tests, where hard steels or carbide balls are pressed above the material surface under specified loads. The BHN is calculated by Equation 9.

$$BHN = 5.970 \times (HRM + 104.7) \quad (9)$$

3.4. Flexural testing

The bending properties of the materials are analyzed by conducting flexural testing (Noryani *et al.* 2019). The FIE – 600KN, C-UTM model is used for this purpose with its ability to hold a maximum load of 600kN. The specimen with a smooth surface is placed between two supports with a loading nose positioned at the center, forming a three-point bending test configuration. The applied load and the corresponding deflections are recorded to measure flexural strength using Equation 10.

$$\sigma_f = \frac{3PL}{2bh^2} \quad (10)$$

where σ_f is the flexural strength with a maximum load at fracture P , and support span lengths L , h , and b signify the height and width of the specimen, correspondingly. The material stiffness is measured by calculating the flexural modulus as Equation (11).

$$E_f = \frac{L^3 m}{4bh^3} \quad (11)$$

where m signifies the slope in the initial straight portions of load-deflection curves.

3.5. Impact testing

The capability of a material to resist high loading or sudden impacts is measured using an impact test (Noryani *et al.* 2020). The SHIVAGANAGA Pendulum Low Impact Energy model is utilized for this study to determine the materials' impact strength. The material behavior under dynamic loading conditions is noted using the impact test. The specimen is placed horizontally in the machine, with the notch facing the pendulum's striking edge. The energy absorbed by the material during fracture is measured by

calculating the variance between the pendulum's first potential energy and the remaining energy after impact, which is measured by the height it reaches after the specimen breakage. The impact energy absorbed by the material is measured by Equation 12.

$$E = mgh_1 - mgh_2 \quad (12)$$

where m denotes the mass of the pendulum, h_1 and h_2 are the height before and after impact. The energy absorbed per unit cross-sectional region at the notch gives impact strength as given by Equation 13.

$$I = \frac{E}{A} \quad (13)$$

where E is the energy absorbed and the cross-sectional area A . This test provides valuable insight into the ductility or brittleness of the material, as ductile materials show greater impact strength with more energy absorbance.

4. Material characterization and degradation analysis

4.1. Biodegradation studies

Biodegradation separates organic material into simpler substances such as water, biomass, or carbon dioxide (Ranganathan and Bojan 2020). This procedure is essential for reducing waste and pollution in the ecosystem. It can occur with or without the involvement of bacteria. In this study, both cases are analyzed. Biodegradation with bacteria involves the breakdown of organic material with the help of microorganisms like bacteria or fungi in aerobic or anaerobic conditions. The effectiveness of these procedures depends upon factors such as pH, temperature, moisture, and nutrient availability. In biodegradation without bacteria, the breakdown of materials through abiotic processes such as photodegradation, oxidation, and thermal degradation are involved. Bacterial degradation is more efficient since it fully mineralizes the material without leaving partially decomposed substances like nonbacterial degradation.

In this study, the weight loss of composites over a period in a nutrient broth environment is evaluated to assess the biodegradability of the samples. Samples were equipped for water absorption measurements by cutting them into 3x1.5 cm strips. The weights of the samples are checked with the initial weight W_0 . Samples were rinsed with distilled water until the wastewater showed a neutral pH. Then, the samples were clamped to glass sheets and dried in vacuum ovens (0.5 mmHg, 50°C ± 2°C, 24 h). The dried films have been located in compost Petri dishes containing 30 mL of NB broth with *Acinetobacter baumannii* and hatched at pH 7.0 ± 0.5, 35°C ± 2°C, and 50% ± 5% relative humidity. After incubation, samples were washed broadly with deionized water and dried; their weight was noted. The weight loss percentage of composites is calculated by Equation 14.

$$\text{weight loss}(\%) = \frac{W_0 - W_1}{W_0} \times 100 \quad (14)$$

4.1.1. Water absorption studies

Water absorption studies assessed the material's potential when exposed to water by analyzing its durability,

degradation, and stability. The test evaluates the ability of a material to absorb water over time. A water absorption test is critical in the context of biodegradable composites since it affects the lifespan and suitability for different applications. Samples for water absorption measurements are prepared by cutting them into 3x1.5 cm strips. The samples were immediately weighed to the adjacent 0.001 g (W_c) after being dried for 8 hours at 50°C ± 2°C in a vacuum oven and cooled in a desiccator. Then, the samples are maintained at 25°C ± 2°C for 6 weeks while immersed in distilled water. During this period, the samples were taken out from the water at 5-day intervals, gently wiped with tissue papers to eliminate excess water from their surfaces, and instantly weighed to the adjacent 0.001 g (W_w), and returned to the water. The % of weight increases owing to water absorption (W_f) was computed to the nearest 0.01% consistent with Equation 15.

$$\text{water absorption}(\%) = \frac{W_w - W_c}{W_c} \times 100 \quad (15)$$

4.2. Fourier transform infrared (FTIR) measurements

FTIR measurements were conducted using an IR Affinity-1 FTIR spectrophotometer from SHIMADZU. The instrument was configured to operate within a spectral range of 400 to 4000 cm^{-1} , suitable for capturing the characteristic absorption bands of various functional groups in the sample. The measurements were taken in % Transmittance mode, providing insights into the molecular structure based on the intensity of light passing through the sample. The instrument was set to a resolution of 4 cm^{-1} , ensuring that fine spectral details were resolved to identify the polymer components accurately. The internal beam configuration and a mirror speed of 2.8 cm/s contributed to the stability and precision of the measurement, allowing for consistent and reproducible results. This setup facilitated the reliable analysis of the sample's molecular composition, aiding in identifying and classifying the polymer through its unique infrared absorption spectrum.

4.3. SEM-EDS analysis

Scanning Electron Microscopy (SEM) analysis at high magnifications investigates a sample's surface morphology and topographical features. With the help of a strong, focused electron beam, the sample's surface is scanned to produce various signals that can be detected and converted into images. Quanta 3D FEG and Nova NanoSEM 450 scanning electron microscopes equipped with TSL-OIM software are used for SEM investigation. The scanning is done at an electron beam resolution of 16 nA at 20 kV. Electrolytic polishing is carried out as part of specimen preparation for SEM using Struers Lectropol-5, a fully automatic electrolytic polishing equipment. The samples were coated with a thin layer of gold to reduce the charging effects under the electron beam. Energy Dispersive X-ray Spectroscopy (EDS) analyses and SEM provide the elemental composition of the sample's specific areas, highlighting the element concentration and distribution across the sample surface. EDS detects the X-rays with different energies corresponding to elements when emitted in conjunction with SEM analysis.

4.4. TG-DT analysis

Thermogravimetric (TG) and Differential Thermal (DT) analysis analyzes the materials' thermal stability, composition, and properties, which is crucial for ensuring better application performance and safety. The degradation patterns obtained from these tests help predict the materials' durability and long life. The thermal stability is measured in terms of weight loss rate as the temperature increases. DT analysis's exothermic and endothermic reactions indicate the phase transitions and crystallization. Coconut, groundnut, and sesame oil wastes are inexpensive agricultural by-products that may be obtained for as little as \$0.30 to \$0.50 per kilogram, which is far less expensive than traditional metallic or asbestos-based fillers. Even while it's still within an industrially acceptable range, the epoxy resin that acts as the matrix somewhat increases the overall cost. There is an estimated 25-30% reduction in the overall manufacturing cost per unit of brake pads compared to traditional pads.

Table 5. Results of tensile strength

Specimen	Tensile Load (KN)	Tensile strength N/mm ²
COR 30% + Epoxy 70%	0.560	11
GOR 30% + Epoxy 70%	1.08	22
SOR 30% + Epoxy 70%	0.780	17
CGS 30% + Epoxy 70%	0.640	12

Table 6. Wear test outcomes

Samples	Initial Weights (g)	Final Weights (g)	Wear Losses (g)
COR	0.297	0.295	0.002
GOR	0.296	0.271	0.025
SOR	0.348	0.341	0.007
CGS	0.365	0.362	0.003

Table 7. Hardness test results

Material	Trail			AVG HRM
COR	20	29	35	28
GOR	34	41	25	33
SOR	25	30	27	27
CGS	45	40	38	41

Table 8. Flexural test results

Samples	Thickness, t (mm)	Span length, l (mm)	Flexural loads, W (KN)	Flexural strength (N/mm ²)
COR 30% + Epoxy 70%	3	150	0.09	75
GOR 30% + Epoxy 70%	3	150	0.12	100
SOR 30% + Epoxy 70%	3	150	0.11	91.7
CGS 30% + Epoxy 70%	3	150	0.08	66.7

Table 5 showcases the effectiveness of the composites to withstand the applied tensile forces. The GOR composite substantially impacts mechanical properties with the highest tensile strength of 22 N/mm². The variations in the tensile strength attributed to differences in composites influence the mechanical properties. The load vs displacement curve for different reinforcements is illustrated in **Figure 6**. **Table 6** shows the results obtained from the wear test analysis.

The wear loss of different samples suggests significant variability in wear resistance, highlighting its durability when performed under friction and abrasion conditions such as brake pads. COR sample shows the lowest wear loss, indicating the high desirability for brake pads since

Compression molding and curing, two common composite fabrication processes, provide the basis of the scalable production process and may be easily integrated into preexisting manufacturing infrastructure with little to no modification. The produced environmentally friendly brake pads also outperform commercially available non-asbestos organic (NAO) pads in terms of mechanical performance, which includes tensile strength, wear resistance, and thermal stability. In addition to being better options from an environmental standpoint, these materials can biodegrade and do not contain any harmful components.

5. Results and discussions

This study analyzed the composites' mechanical properties and spectroscopic characteristics to assess the suitability of the selected materials for brake pad applications.

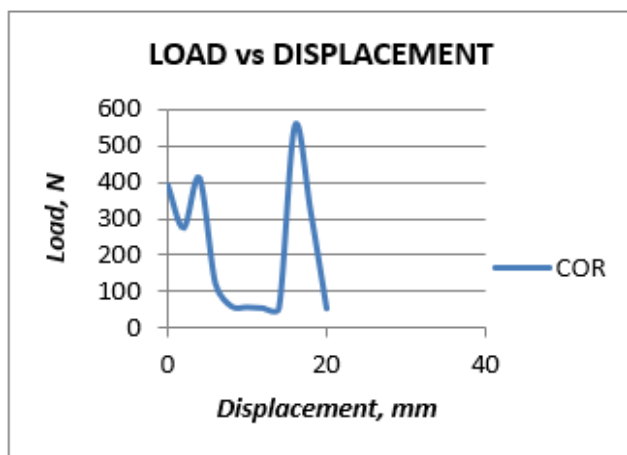
5.1. Evaluation of mechanical properties

they are wearing resistant, contributing to long-lasting performance. Moreover, materials having low wear loss demonstrate higher durability, making them suitable for harsh braking conditions. **Figures 7 to 10** illustrate the relationship of time with wear, frictional force, and coefficient of friction for various reinforcements, emphasizing the necessity of managing friction and thermal effects to enhance the material performance for brake pads. Biodegradation studies were carried out under controlled laboratory composting settings utilizing *Acinetobacter baumannii* to evaluate the microbial breakdown behavior of the proposed brake pad composites. To mimic the circumstances of natural biodegradation, the process included creating soil compost

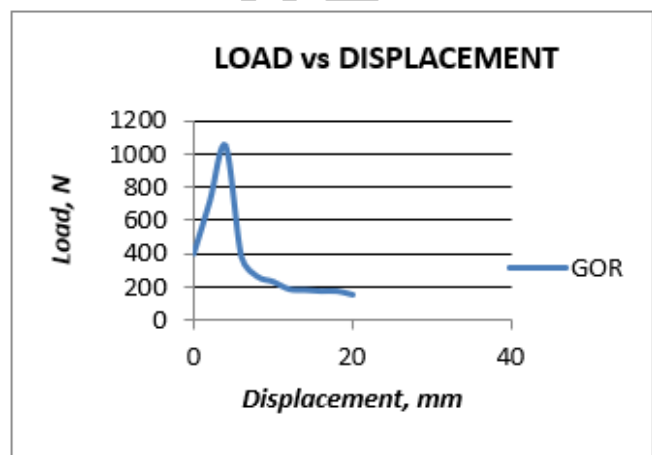
habitats that were supplemented with cultures of *Acinetobacter baumannii* at a predetermined concentration. These settings were kept at 30–35°C and relative humidity of 60–70%. For 30, 60, and 90 days, specimens of the brake pad were buried in a compost matrix after being chopped into uniform dimensions (e.g., 30 mm × 30 mm × 5 mm). To determine the proportion of material decomposed over time, specimens were meticulously removed at each interval, rinsed to remove exterior compost residues, dried, and then measured for weight loss.

The application of materials for brake pads requires high resistance to deformations. CGS shows the highest average hardness with 41 HRM in the combined residue sample. The GOR material follows with a value of 33 HRM, offering good hardness, suitable for moderately demanding applications. **Table 8** provides the results of the flexural test. Executed under ASTM D638 guidelines utilizing a Universal Testing Machine (UTM). The samples were shaped like a dog bone with a 50 mm gauge length. A

constant speed of 5 mm/min was maintained for the crosshead. The ductility and tensile strength were determined by recording the highest tensile force and elongation at break. Performed in a three-point bending setup following ASTM D790. Over a 60 mm span, rectangular specimens measuring 80 mm × 12.7 mm × 6 mm were held in place. The maximum load that could be applied before fracture was used to calculate the flexural strength, and a 2 mm/min loading rate was used in the experiment. Impact testing was performed according to ASTM D256 using the Izod technique. Specimens that were notched and had dimensions of 63.5 mm × 12.7 mm × 6 mm were utilized. We recorded the impact energy absorbed before fracture to measure toughness and energy absorption capacity. The durometer was set up in compliance with ASTM D2240 to measure the Shore D hardness. To be sure the samples were all the same, we took several measurements from each surface and averaged them.



(a) COR



(b) GOR

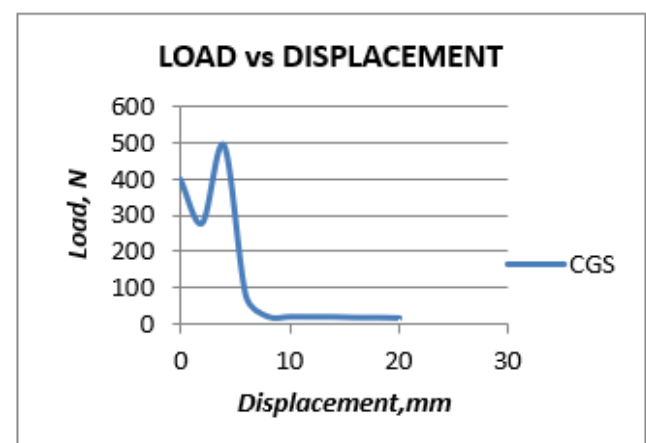
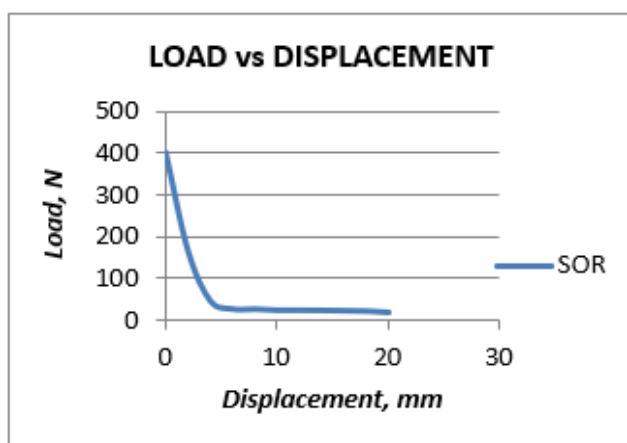


Figure 6. Load vs Displacement curve

Surface hardness indicates how well a material resists localized plastic deformation. A pin-on-disc tribometer, designed according to ASTM G99, was used to conduct dry sliding wear tests. The test parameters were a total sliding distance of 1500 m, a track diameter of 100 mm, a speed

of 1.5 m/s, and a load of 20 N. We determined wear loss by comparing the specimen's weight before and after testing. Worked according to ASTM D570 specifications. After drying, the specimens were placed in distilled water and left at room temperature for 24, 48, and 72 hours of

immersion. We assessed the moisture absorption capacity, which determines long-term dimensional and mechanical stability, by measuring the weight growth at each interval. From **Table 8**, GOR samples provide the highest flexural strength at 100 N/mm², indicating that it can withstand greater bending force before failure, making it suitable for brake pads, as they require strong and rigid materials. The

SOR sample follows with 91.7 N/mm², suggesting substantial resistance to bending. **Table 7** provides the results of the impact test. The energy absorption capacity of different composites is represented in terms of impact values.

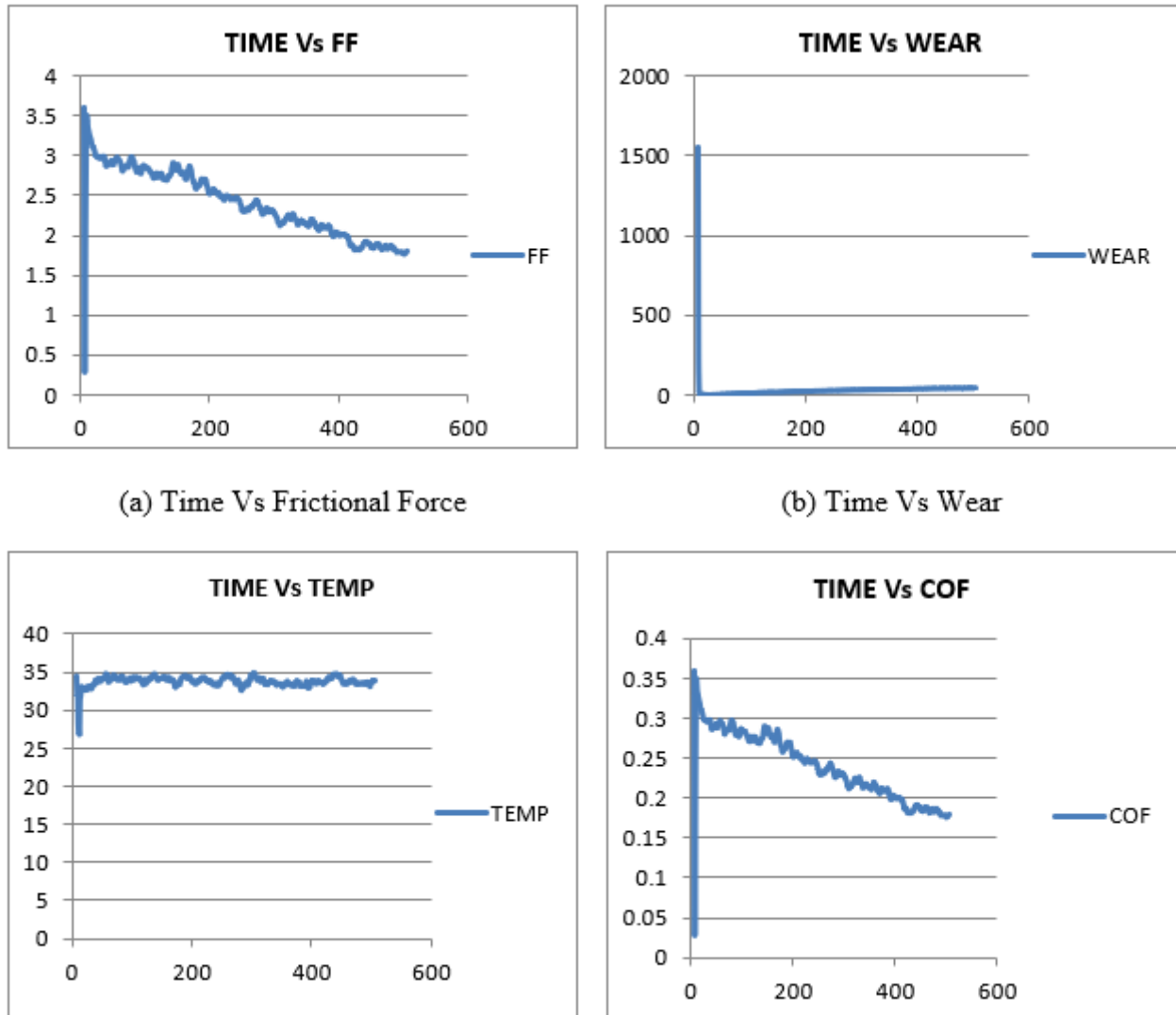


Figure 7. Time-dependent wear test results for COR sample

Table 9. Impact test results

Samples	Impact values (J)
COR 30% + Epoxy 70%	3
GOR 30% + Epoxy 70%	1.8
SOR 30% + Epoxy 70%	2.6
CGS 30% + Epoxy 70%	1.2

The coconut oil residue shows high energy absorption with an impact value of 3J. The value suggests the ability of the composite to resist sudden forces, offering better toughness. The environmentally friendly brake pads' thermal stability and degrading behavior were illuminated by the results of the Thermogravimetric study (TGA) thermal study. Organic composite materials typically decompose in three stages, as the TGA curve shows. The first, small weight loss (about 4-6% of the total) was caused by the volatilization of low-molecular-weight molecules

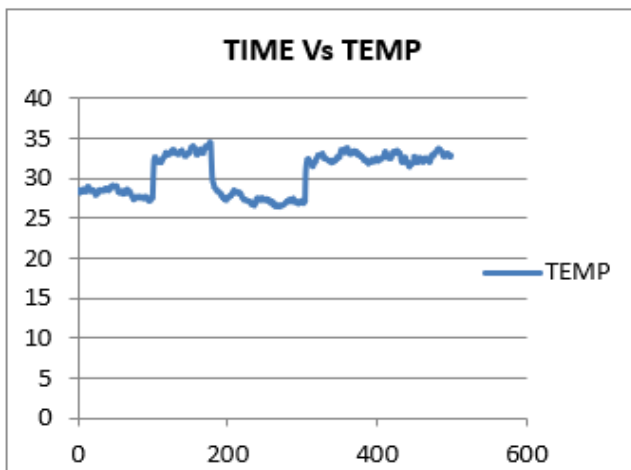
and the desorption of moisture. This step verifies that the composite retains very little moisture to avoid thermal breakdown too soon during braking. During this stage, the lignocellulosic components (hemicellulose and cellulose) found in the coconut, groundnut, and sesame leftovers exhibited the greatest weight reduction (around 45-52%). The composite's thermal resistance threshold, about 280°C, falls well within the working temperature range of automobile braking systems, which usually operate between 100 and 250°C. This guarantees that the brake pads will not collapse under the normal braking heat loads or reduce their performance. The progressive mass loss was attributed to degrading the epoxy matrix and remaining carbonaceous elements. As a result of a solid carbon backbone construction, the thermal shielding effect is improved and heat is dissipated during braking events, as shown by the final residual char content of around 20-25%.

5.2. Evaluation of material characterization and degradation analysis

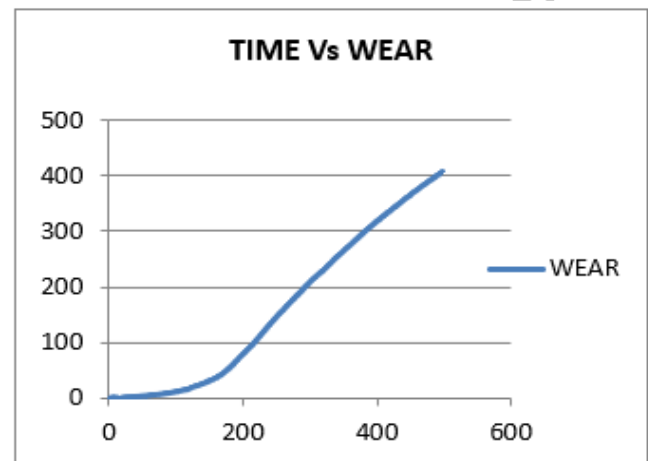
The spectroscopy of biodegradation with and without bacteria is illustrated in **Figure 11**.

When exposed to bacteria, the SEM images show the effects of biodegradation on different oil residues (CGS, COR, GOR, and SOR). The comparison between the images with and without bacteria reveals distinct differences in surface morphology, indicating varying degrees of biodegradation. The samples exposed to bacteria exhibit more pronounced surface roughness, pitting, and microvoids than the relatively smoother surfaces of the

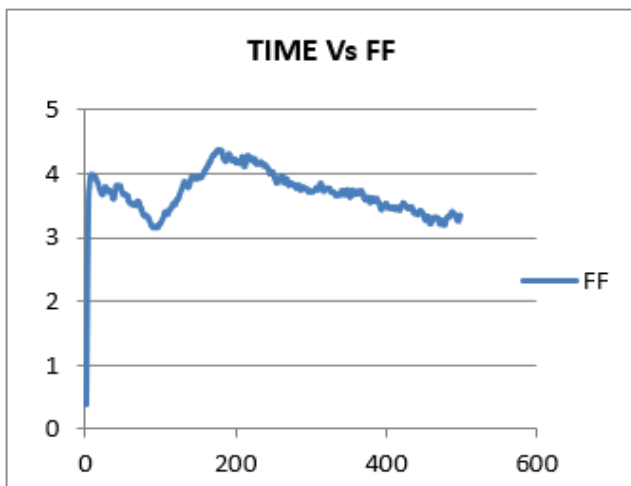
control samples without bacteria. For example, in the CGS and COR samples, the bacterial activity significantly altered the surface texture, suggesting higher biodegradation. In contrast, the GOR and SOR samples show less pronounced changes, indicating potentially lower biodegradability. This suggests that the biodegradation rate and effectiveness differ among the oil residues, with CGS and COR being more susceptible to bacterial breakdown, making them potentially eco-friendly and more suitable for applications where biodegradability is a desired characteristic.



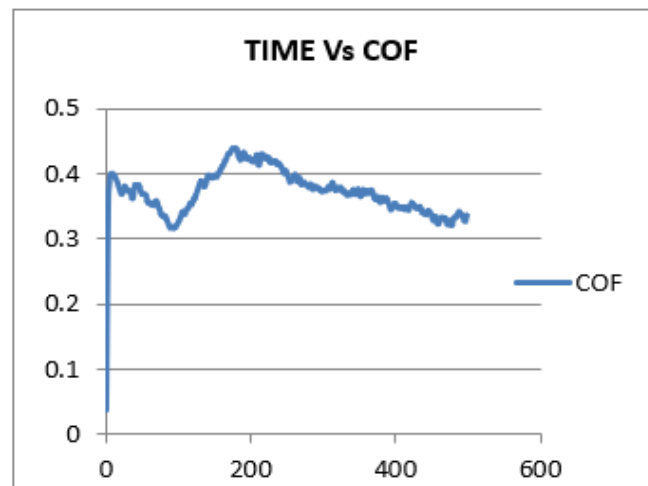
(a) Time Vs Temp



(b) Time Vs Wear



(c) Time Vs Frictional Force



(d) Time Vs COF

Figure 8. Time-dependent wear test results for GOR sample

The water absorption studies showing weight changes of the four samples over six weeks are illustrated in **Table 10**. The % change indicates the weight change from the initial stage to the sixth week.

Underwater absorption, the SOR sample shows minimal variation in weight, demonstrating its stability with minimal reaction to the conditions over time. The COR sample follows with relatively stable characteristics under the given conditions. This study provides insight into the material stability to maintain the characteristics over time.

Table 11 shows the results of biodegradation studies. There is a considerable decrease in the environmental impact during sourcing when agricultural by-products such as coconut, peanut, and sesame oil leftovers are used. Asbestos and other traditional materials are extracted and processed using much energy, yet these leftovers are waste products with almost no environmental effect. Combining them with waste valorization and circular economy concepts is a win-win. The production uses low-energy processes like compression molding, resin mixing, and

particle processing. Approximately 20-25% less energy is required, resulting in lower cumulative energy demand (CED) and fewer greenhouse gas emissions (0.8-1.2 kg CO₂ equivalent per brake pad) when compared to traditional methods of making brake pads, which involve high-temperature sintering and heavy metal reinforcement. While vehicles operate, vehicles operate, standard pads emit toxic brake dust, including heavy metals and synthetic particles. Based on the EDS and FTIR analyses, the created pads do not emit harmful substances and generate less harmful particulate matter, making them safer for the environment and the air. Results from 30 days of

biodegradation tests using *Acinetobacter baumannii* under composting settings showed a 28-35% mass loss, suggesting efficient microbial breakdown. Negligible biodegradability means that pads made of asbestos or synthetic materials will stay in landfills for a very long time, adding to environmental contamination. The absence of harmful by-products throughout the degrading process further assures that disposal will not harm the environment.

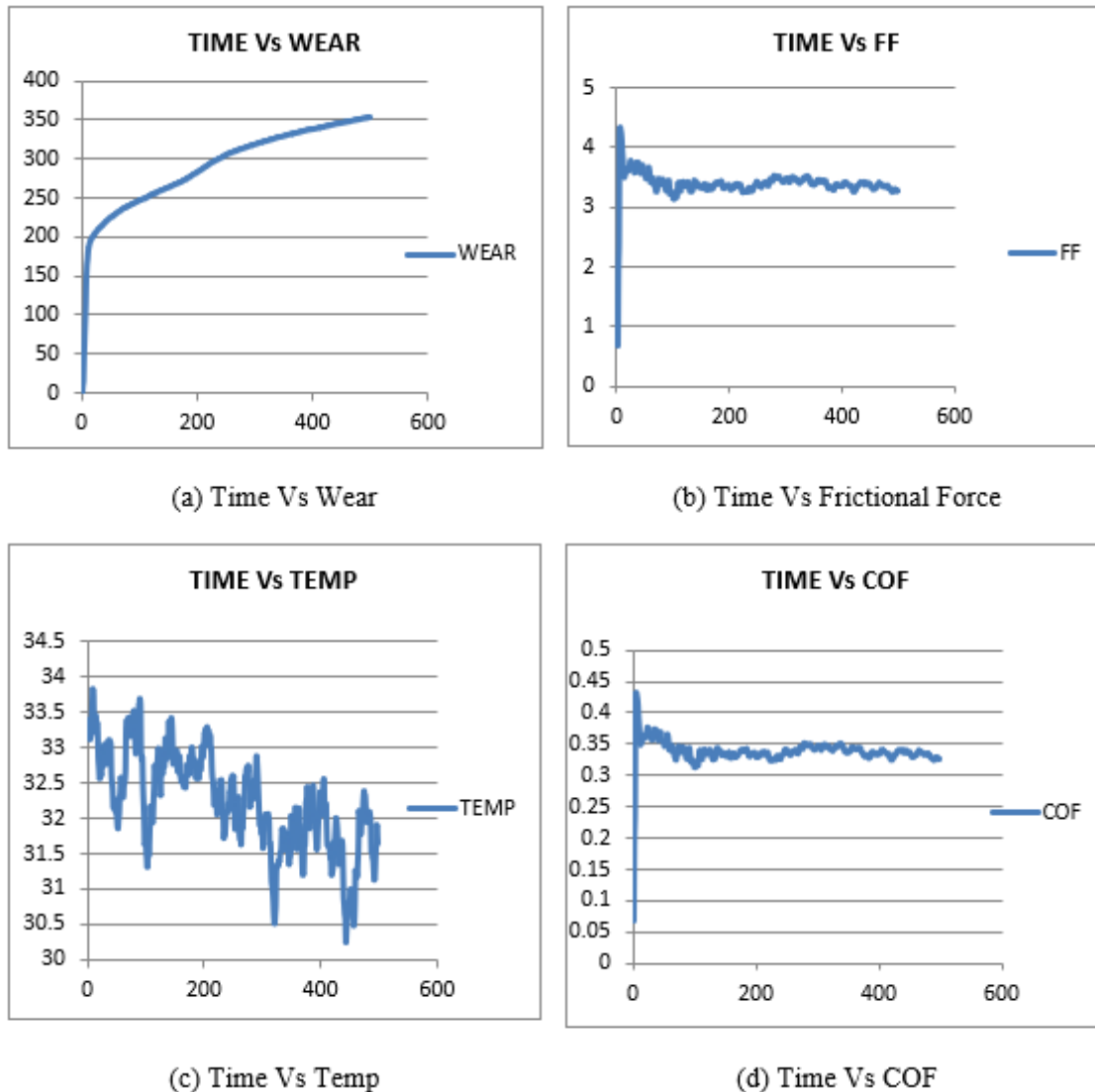


Figure 9. Time-dependent wear test results for SOR sample

Table 11 demonstrates the weight loss percentage, highlighting the effectiveness of the oil residues under biodegradation. GOR is the most biodegradable material, with 13.8816 % weight loss. EDX analysis investigates the nearness and availability of various elements in the oil residue composites to provide valuable insights into their uniformity and compositions. **Figure 15** represents EDX images of various oil residue composite compositions. The proposed oil residue-based brake pad materials exhibit considerable environmental benefits over traditional materials regarding both carbon footprint and toxicity. Life

cycle assessment (LCA) estimates indicate a carbon footprint reduction of approximately 30–40% compared to conventional asbestos or metallic-based pads, primarily due to the renewable origin and lower embodied energy of agricultural waste fillers. Processing natural residues requires less thermal and mechanical energy, contributing to lower CO₂ emissions across the manufacturing chain. Regarding toxicity, traditional pads often contain heavy metals (e.g., antimony, copper, lead) and asbestos, which release hazardous particulate matter during wear and pose serious health risks. In contrast, the proposed materials'

elemental analysis (EDS) confirms the absence of toxic elements, and no harmful leachates were observed during degradation.

Table 10. Water absorption studies

Sample	Weight (g)							% Change
	Initial	1st Week	2nd Week	3rd Week	4th Week	5th Week	6th Week	
COR	1.164	1.272	1.203	1.179	1.177	1.177	1.176	1.03
GOR	1.250	1.294	1.310	1.303	1.303	1.302	1.301	4.08
SOR	1.217	1.265	1.230	1.225	1.225	1.224	1.224	0.57
CGS	1.195	1.258	1.266	1.271	1.271	1.276	1.275	6.69

Table 11. Percentage of weight loss

Sl. No.	Samples	Test Percentage of Weight Loss (%)	Control Percentage of Weight Loss (%)
1	COR	3.3056%	0.5303%
2	GOR	13.8816%	0.267%
3	SOR	2.5094%	0.0799%
4	CGS	4.5284%	0.223%

The composition of the oil residue materials was analyzed to evaluate the suitability of the brake pad's characteristics. The COR exhibits lower carbon content (56.44%) compared to SOR (62.76%), suggesting that SOR offers superior performance of frictional properties. COR's high nitrogen and oxygen content affects the stability and wear resistance. Additionally, with high carbon and balanced oxygen and nitrogen content, SOR provides high durability and friction, making it the ideal option for brake pad application. Lightweight commercial vehicles were subjected to a pilot-scale field test utilizing the newly designed environmentally friendly brake pads to corroborate the laboratory results. Braking efficiency, wear

rate, temperature resistance, and noise levels were major performance parameters tested across more than 5,000 km of urban and semi-urban road settings. The environmentally friendly brake pads showed consistent braking performance, on par with commercially available non-asbestos organic (NAO) pads, with an average 3% variance in stopping distance. According to the wear rate measurements, the material loss was consistently within acceptable industrial norms, and the thermographic examination revealed no anomalous heat accumulation even after many braking cycles.

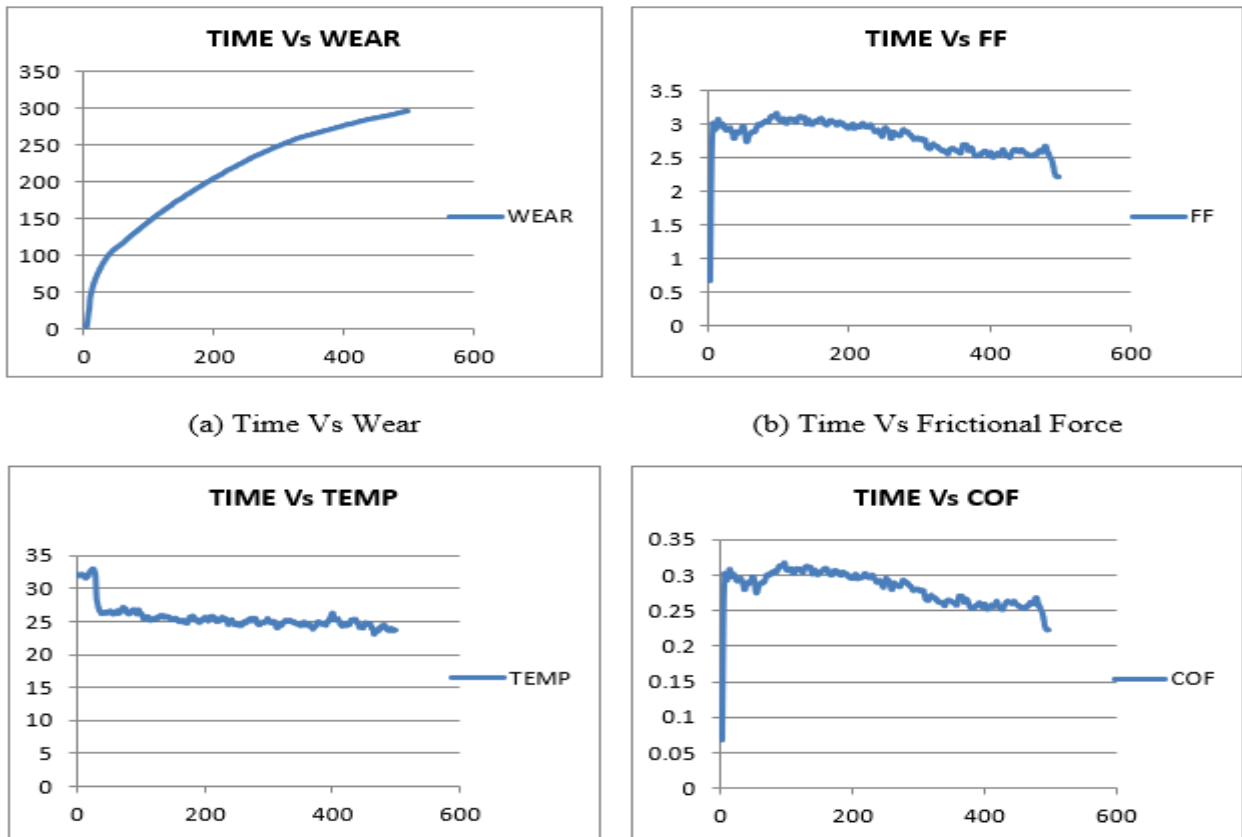


Figure 10. Time-dependent wear test results for CGS sample

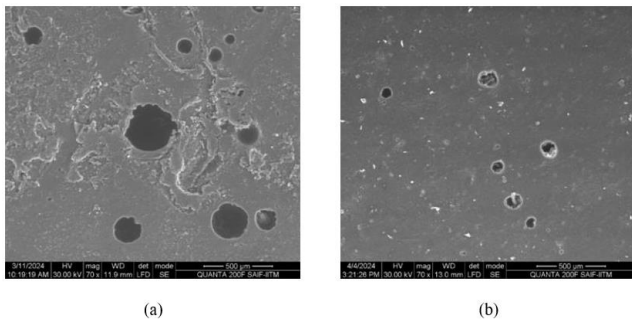


Figure 11. Spectroscopy of biodegradation of CGS sample (a) with bacteria (b) without bacteria

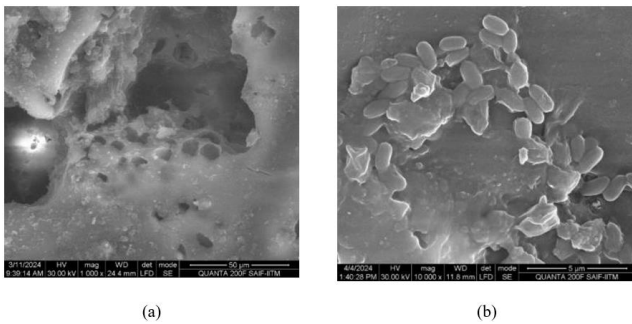


Figure 12. Spectroscopy of biodegradation of COR sample (a) with bacteria (b) without bacteria.

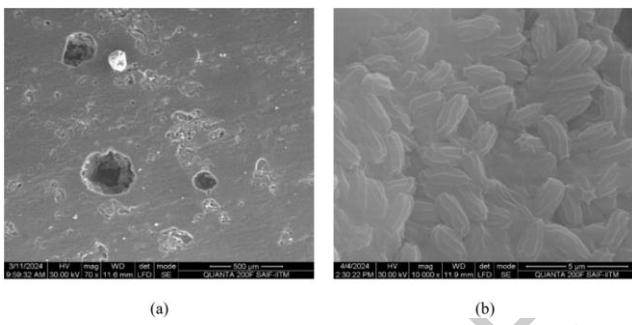


Figure 13. Spectroscopy of biodegradation of GOR sample. (a) with bacteria (b) without bacteria.

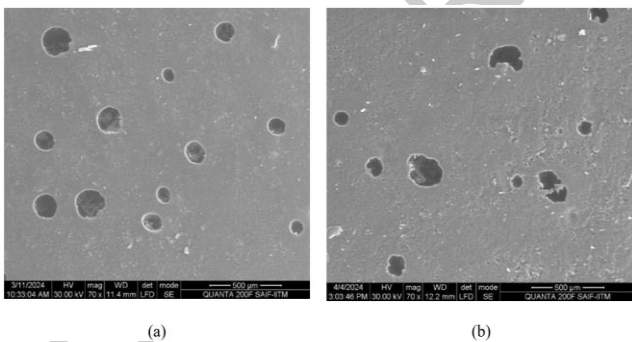


Figure 14. Spectroscopy of biodegradation of SOR sample (a) with bacteria (b) without bacteria.

The importance of surface texture in selecting the most promising material for brake pad application is evaluated through SEM analysis. The surface morphology of various oil residues directly influences their performance. COR exhibits a relatively smooth surface with distinct features, suggesting a less complex microstructure. GOR shows a rougher surface with more pores, whereas CGS displays a composite nature, enhancing the interaction with other materials. These morphological changes had a greater impact on wear resistance and biodegradability and are suitable for brake pad applications. Unpredictability in raw

material quality, processing uniformity, and supply chain stability are potential obstacles to increasing manufacturing of these environmentally friendly brake pads. Oil leftovers such as sesame, peanut, and coconut may compromise composite property consistency at the industrial scale, which can display batch-to-batch variations in fiber composition, moisture content, and particle size. Process optimization and equipment calibration may be necessary to maintain uniform filler-matrix dispersion during high-volume mixing and molding. Also, there can be supply chain issues since the availability of these residues might vary by season or area, even if they are agricultural by-products. Regarding large-scale operations, factors like epoxy curing periods and heat management may impact production throughput and cost efficiency. Additionally, considerable testing and validation cycles may be necessary for regulatory approval and performance standards in automotive applications, which might postpone market introduction.

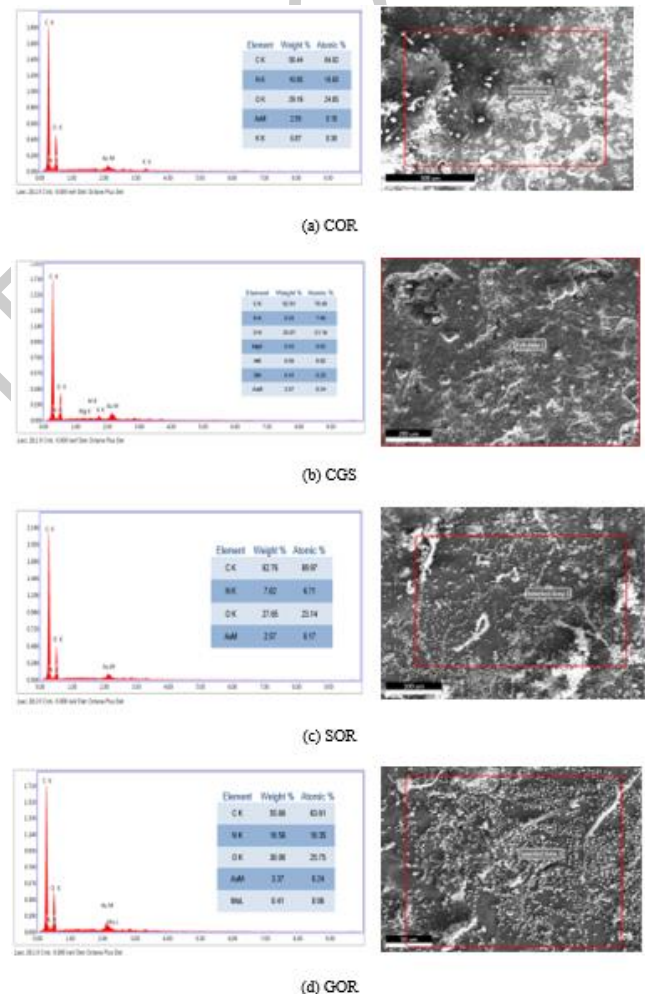


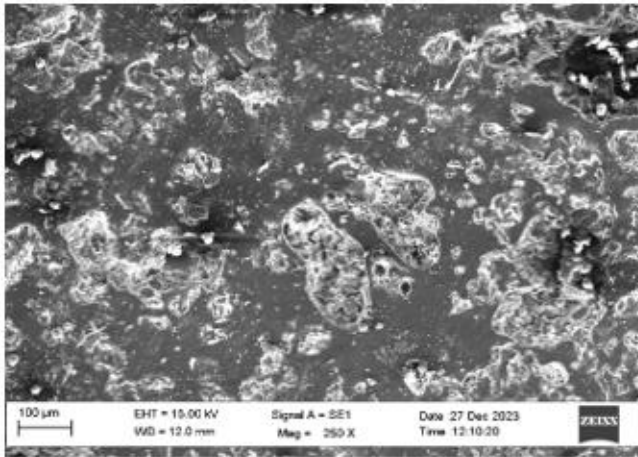
Figure 15. EDX analysis of various oil residue compounds.

The thermal behavior of four different oil residues is evaluated using TG/DTA Analysis. The TG curve in **Figure 17** shows the multi-step degradation process and weight loss under different temperature levels, whereas the DTA curve indicates the endothermic and exothermic peaks reflecting complex thermal events such as melting, crystallization, and decomposition. The combination residue, CGS, demonstrates complex thermal patterns similar to COR with multiple transitions. GOR and SOR provide stable

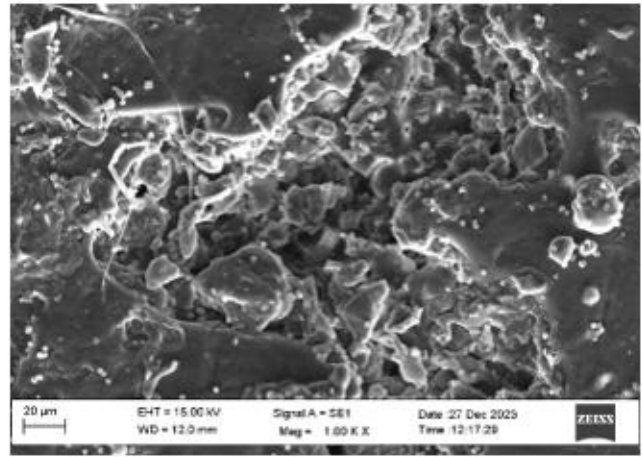
thermal behavior, making them suitable for brake pad applications.

Mechanical parameters (hardness, flexural strength, tensile strength, and impact resistance) were compared among groundnut, coconut, and sesame-based composites using one-way analysis of variance. The findings supported statistically significant variations ($p < 0.05$) in critical

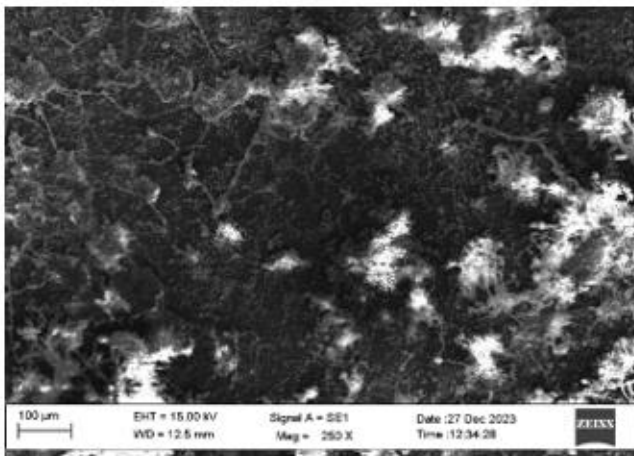
parameters, further demonstrating that the kind of filler affects the performance of the composite. Also, this study used Pearson's correlation analysis to examine how mechanical, biodegradation and thermal properties were related; this study found that filler dispersion positively correlated with biodegradation rate and thermal stability.



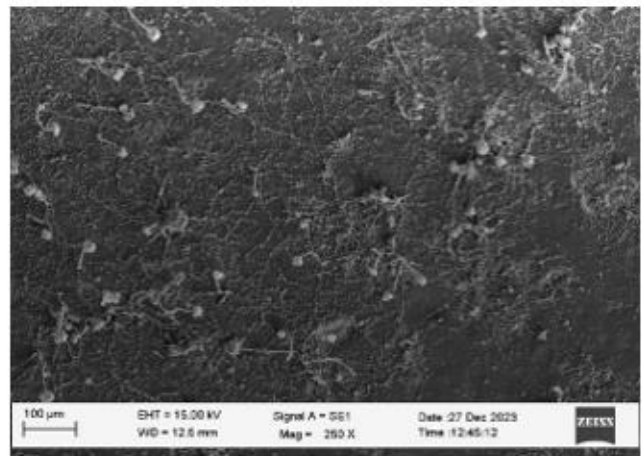
(a) COR



(b) CGS



(c) SOR



(d) GOR

Figure 16. SEM analysis of oil residue composites.

6. Conclusion

The feasibility of using eco-friendly materials derived from natural fibers sourced from the residue of the oil extraction process is successfully investigated in this study. Using agricultural oil wastes as reinforcement, such as coconut, groundnut, and sesame oil, helps to fit the concepts of the circular economy and waste valorization by reducing reliance on non-renewable and dangerous fillers like asbestos and heavy metals. Secondly, unlike traditional synthetic pads, which cannot be biodegraded, experiments including *Acinetobacter baumannii* in composting environments demonstrated a 28-35% mass loss after 30 days, suggesting substantial microbial degradability. Thirdly, since natural fillers mainly demand less energy during manufacturing, eco-friendly pads have a life cycle energy intake of about 20-25% lower than conventional

brake pads. The oil residues of coconut, ground nut, sesame, and combination are incorporated with epoxy resin with different reinforcement ratios to fabricate brake pads. The mechanical properties of the samples were evaluated under ASTM standards through tensile strength, wear resistance, hardness, flexural strength, and impact resistance tests. The SEM-EDS results demonstrated that the brake pads reinforced with oil residues meet the high demand of automotive applications. Additionally, biodegradation tests without and with bacteria such as *Acinetobacter baumannii* compost and its morphological surface represent their capability to break down and thus minimize environmental impact. Overall, the study outcomes indicate that the oil residues, often considered a waste product, can effectively manufacture sustainable and eco-friendly brake pads cost-effectively.

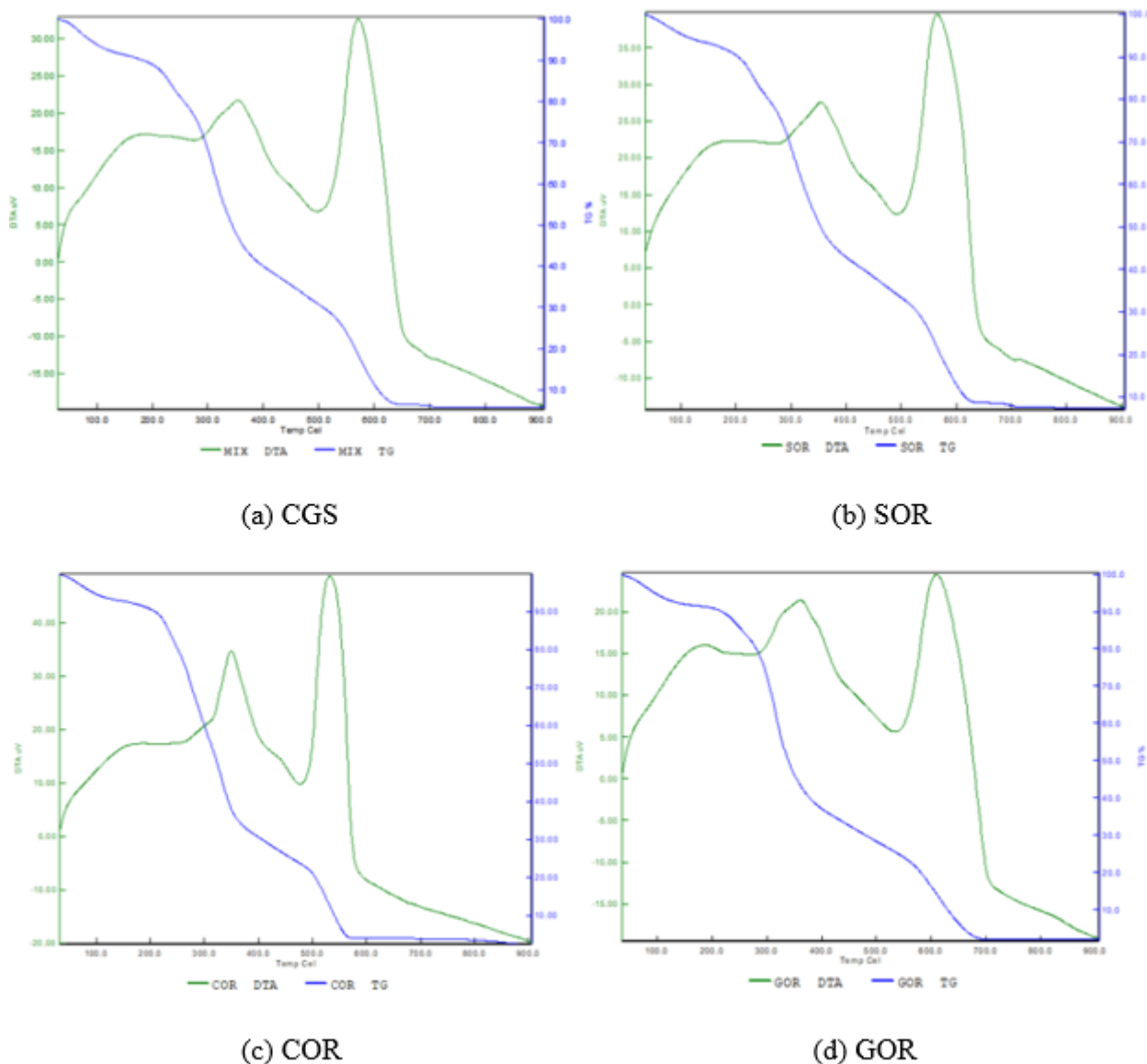


Figure 17. TG/DTA Analysis

References

- Allasi, H. L., Rajalingam, A. A., Jani, S. P. and Uppalapati, S. (2023). Influence of synthesized (green) cerium oxide nanoparticle with neem (*Azadirachta indica*) oil biofuel. *Bulletin of the Chemical Society of Ethiopia*, **37**(2), 477–490.
- Ammar Z., Ibrahim H., Adly M., Sarris I., and Mehanny S. (2023). Influence of natural fiber content on the frictional material of brake pads—a review, *Journal of Composites Science*, **7**, 72.
- Arul, S. J., Basavaraj, N. M. and SP, J. (2024). Influence of bio fillers on the characteristics of *Luffa acutangula* fiber reinforced polymer composites and parametric optimization using Taguchi technique. *Scientific Reports*, **14**(1), 30730.
- Arul, S. J., Jani, S. P., Adhikary, P. and Lenin, A. H. (2024). Effect of chemical treatments of fibre surface on mechanical properties and wear rate of Beerakaya (*Luffa acutangula*) reinforced epoxy polymer composites. *Polymer Bulletin*, 1–20.
- Balakrishnan E., Meganathan S., Balachander M., and Ponshanmugakumar A. (2019). Elemental analysis of brake pad using natural fibres, *Materials Today: Proceedings*, **16**, 1067–1074.
- Dharmakrishnan S., Pandian P., and Sembian M. (2022). Sustainable characterization of silane treated and untreated *Psidium guajava* stem natural fibers based automobile brake pads, *Journal of Natural Fibers*, **19**, 7982–7995.
- Ekpruke E.O., Ossia C.V., and Big-Alabo A. (2023). On the Morphological and Tribological Characterization of Green Automotive Brake Pads Developed from Waste This Coronata Seashells, *Jordan Journal of Mechanical & Industrial Engineering*, **17**.
- Eziwhuo S.J., Ossia C.V., and Joseph T. (2023). Characterization of produced biodegradable brake-pad from waste coconut fruit fiber and oyster sea shells as reinforcement materials, *Journal of Manufacturing Engineering*, **18**, 043–057.
- Hemlata. and Maiti S.N. (2015). Mechanical, morphological, and thermal properties of nanotalc reinforced PA6/SEBS-g-MA composites, *Journal of Applied Polymer Science*, **132**.
- Irawan A.P., Fitriyana D.F., Tezara C., Siregar J.P., Laksmidewi D., Baskara G.D., and Najid N. (2022). Overview of the important factors influencing the performance of eco-friendly brake pads, *Polymers*, **14**, 1180.

- Khafidh M., Putera F.P., Yotenka R., Fitriyana D.F., Widodo R.D., Ismail R., and Ismail N.H. (2023). A study on characteristics of brake pad composite materials by varying the composition of epoxy, rice husk, Al₂O₃, and Fe₂O₃, *Automotive Experiences*, **6**, 303–319.
- Kumar N., Mehta V., Kumar S., Grewal J.S., and Ali S. (2022). Bamboo natural fiber and PAN fiber used as a reinforced brake friction material: developed asbestos-free brake pads, *Polymer Composites*, **43**(5), 2888–2895.
- Kumaravel, S., Saravanan, C. G., Vikneswaran, M., Raman, V., Sasikala, J., Js, F. J. and Allasi, H. L. (2024). Exploration of flame characteristics of gasoline engine fuelled by gasoline-pentanol blends using combustion endoscopy. *Scientific Reports*, **14**(1), 31692.
- Kunaroop N., Rimdusit S., Mora P., Hiziroglu S. and Jubsilp C. (2024). Carbonized hemp hurd powder for eco-friendly polybenzoxazine composite brake material: Excellent friction property and high mechanical performance, *Arabian Journal of Chemistry*, **17**, 105769.
- Li, Y., Cong, R., Zhang, K., Ma, S. and Fu, C. (2024). Four-way game analysis of transformation and upgrading of manufacturing enterprises relying on industrial internet platform under developers' participation. *Journal of Asian Architecture and Building Engineering*, 1–22.
- Ma, S. W. L. Y. Y., Wang, L. and Yuan, Y. (2024). Study on the coupled and coordinated development of tourism, urbanization and ecological environment in shanxi province. *Global NEST Journal*, **26**(4), 10-30955.
- Murugan, S. and Arul, S. J. (2024). A Novel Real-time assessment of the wear analysis of Cu-Ni-Sn hybrid composite for multi-functional applications strengthened by nano B 4 C. *Archives of Metallurgy & Materials*, **69**(3).
- Naidu M., Bhosale A., Munde Y., Salunkhe S., and Hussein H.M.A. (2022). Wear and friction analysis of brake pad material using natural hemp fibers, *Polymers*, **15**, 188.
- Naidu M., Bhosale A., Munde Y., Salunkhe S., and Hussein H.M.A. (2022). Wear and friction analysis of brake pad material using natural hemp fibers, *Polymers*, **15**, 188.
- Nandiyanto A.B.D., Fitriani A.F., Pradana R.A., Ragadhita R., Azzaoui K., and Piantari E. (2024). Green Innovation in Brake Pad Production: Harnessing Teak Powder and Clam Shells as Sustainable Alternatives for Subtractive Residual Waste, *Moroccan Journal of Chemistry*, **12**, 714–733.
- Noryani M., Sapuan S.M., Mastura M.T., Zuhri M.Y.M., and Zainudin E.S. (2019). Material selection of a natural fibre reinforced polymer composites using an analytical approach, *Journal of Renewable Materials*, **7**, 1165–1179.
- Noryani M., Sapuan S.M., Mastura M.T., Zuhri M.Y.M., and Zainudin E.S. (2020). Statistical inferences in material selection of a polymer matrix for natural fiber composites, *Polimery*, **65**, 105–114.
- Ranganathan S., and Bojan S.G. (2020). Tribological behaviour of carbon fibre reinforced biodegradable material as an alternative frictional brake pad in automobiles, No. 2020-28-0513, SAE Technical Paper.
- Saravanan, C. G., Varuvel, E. G., Vikneswaran, M., Femilda Josephin, J. S., Chinnathambi, A., Pugazhendhi, A. and Allasi, H. L. (2024). The combustion of lemon peel oil/gasoline blends in spark ignition engine with high-insulation piston crown coating. *Scientific Reports*, **14**(1), 28740.
- Shen, D., Guo, X. and Ma, S. (2024). Study on the Coupled and Coordinated Development of Climate Investment and Financing and Green Finance of China. *Sustainability*, **16**(24), 11008.
- Singh T. (2024). An integrated multicriteria decision making framework for the selection of waste cement dust filled automotive brake friction composites, *Scientific Reports*, **14**, 6817.
- Sutikno S., Pramujati B., Safitri S.D., and Razitania A. (2018). Characteristics of natural fiber reinforced composite for brake pads material, In: AIP Conference Proceedings, Vol. 1983, No. 1, AIP Publishing.
- Tong, L., Wang, C., Qi, Q., Ma, S. and Mei, J. (2024). Study on the impact of China's digital economy on agricultural carbon emissions. *GLOBAL NEST JOURNAL*, **26**(6).
- Wang, C., Liu, H. and Ma, S. (2024). Analysis of the effect of digital financial inclusion on agricultural carbon emissions in China. *GLOBAL NEST JOURNAL*, **26**(8).
- Wang, Z., Wang, F. and Ma, S. (2024). Research on the Coupled and Coordinated Relationship Between Ecological Environment and Economic Development in China and its Evolution in Time and Space. *Polish Journal of Environmental Studies*.
- Wang, Z., Wu, Q. and Ma, S. (2024). Research on carbon emission peaks in large energy production region in China-Based on the open stirpat model. *Global NEST Journal*, **26**(5).
- Wen, L., Ma, S. and Lyu, S. (2024). The influence of internet celebrity anchors' reputation on consumers' purchase intention in the context of digital economy: from the perspective of consumers' initial trust. *Applied Economics*, **56**(60), 9189–9210.
- Wen, L., Ma, S. and Su, Y. (2024). Analysis of the interactive effects of new urbanization and agricultural carbon emission efficiency. *Global NEST Journal*, **26**(4).
- Wen, L., Ma, S., Wang, C., Dong, B. and Liu, H. A Study of Green Strategy Choice and Behavioral Evolution of Consumers and Producers under the Double Subsidy Policy. *Polish Journal of Environmental Studies*.
- Wen, L., Ma, S., Zhao, G. and Liu, H. (2025). The Impact of Environmental Regulation on the Regional Cross-Border E-Commerce Green Innovation: Based on System GMM and Threshold Effects Modeling. *Polish Journal of Environmental Studies*, **34**(2).
- Wu, Q., Jin, Y. and Ma, S. (2024). Impact of Dual Pilot Policies for Low-Carbon and Innovative Cities on the High-Quality Development of Urban Economies. *Global NEST Journal*, **26**(9), 10-30955.
- Wulansari I., Aume D.P.P., Seprianto M., Aryanti F.I., and Prayudie U. (2024). Development of Brake Camp Material Using Reinforced Polymer Composite by Clamshells/Cardboard Waste/Orange Peel, *Jurnal Inotera*, **9**, 178–183.
- Xia, W., Ruan, Z., Ma, S., Zhao, J. and Yan, J. (2025). Can the digital economy enhance carbon emission efficiency? Evidence from 269 cities in China. *International Review of Economics & Finance*, **97**, 103815.
- Yao, B., Li, C. and Huang, R. (2024). Study on the Dynamic Analysis of the Evolutionary Game and Influence Effect of Green Taxation in Promoting the Development of New Energy Industry. *Journal of Comprehensive Business Administration Research*.

- Yigrem M., Fatoba O., and Tensay S. (2022). Tensile strength, wear characteristics and numerical simulation of automotive brake pad from waste-based hybrid composite, *Materials Today: Proceedings*, **62**, 2954–2964.
- Zeng, H., Abedin, M. Z., Lucey, B. and Ma, S. (2025). Tail risk contagion and multiscale spillovers in the green finance index and large US technology stocks. *International Review of Financial Analysis*, **97**, 103865.
- Zhang, K., Li, Y., Ma, S. and Fu, C. Research on the Impact of Green Technology Innovation in the Manufacturing Industry on the High-Quality Development of the Manufacturing Industry Under “Dual Circulation”. *Polish Journal of Environmental Studies*.
- Zou, F., Ma, S., Liu, H., Gao, T. and Li, W. (2024). Do technological innovation and environmental regulation reduce carbon dioxide emissions? evidence from China. *Global NEST Journal*, **26**(7).

UNCORRECTED PROOFS